Interaction of Dioxygen with Al Clusters and Al(111): A Comparative Theoretical Study

C. Mosch,[†] C. Koukounas,[‡] N. Bacalis,[§] A. Metropoulos,[§] A. Gross,*[,†] and A. Mavridis*[,‡]

Institute for Theoretical Chemistry, Ulm University, D-89069 Ulm, Germany, Laboratory of Physical Chemistry, Department of Chemistry, National and Kapodistrian University of Athens, P.O. Box 64004, 157 10 Zografou, Athens, Greece, and Theoretical and Physical Chemistry Institute, National Hellenic Research Foundation, Athens 11635, Greece

Received: December 21, 2007; In Final Form: February 17, 2008

We have studied the interaction of an oxygen molecule with Al clusters and Al(111) using both wave-function-based quantum chemistry methods and density functional theory (DFT). These calculations were motivated by the fact that molecular beam experiments indicate that the adsorption of O_2 on Al(111) should be activated whereas periodic DFT calculations yield purely attractive adsorption paths for almost all impact configurations of O_2 on Al(111). On small Al_4 clusters, accurate wave-function-based quantum chemistry methods find a non-vanishing barrier in the O_2 adsorption. The DFT calculations for slabs and larger Al clusters confirm the important role of spin effects for the O_2 dissociation barrier on Al. The results indicate that exchange-correlation effects play a crucial role for the determination of the adsorption barrier in the O_2/Al system but their determination is hampered by serious technical problems that are discussed in detail.

I. Introduction

Understanding how geometry and electronic structure affect reactivity is essential to such diverse areas as thin film coating, catalysis, and corrosion. In particular, the interaction of oxygen with metal particles and surfaces is of tremendous technological importance because oxidation reactions are ubiquitous in heterogeneous catalysis. The most prominent example is the car exhaust catalyst[1] in which carbon monoxide and other toxic gases are converted into less-harmful products. The activation of oxygen, that is, the dissociative adsorption of O_2 on the catalyst, is one of the crucial reaction steps occurring in the car exhaust catalyst where the catalytic active material is mainly platinum. However, in spite of the technological relevance of these systems, the exact microscopic mechanism of this fundamental reaction on low-index surfaces of Pt is still debated.[2,3] For another seemingly simple system in this context, the interaction of O_2 with Al(111), a generally accepted picture of the dissociation dynamics is still missing. Although molecular beam experiments suggest that the adsorption is hindered by a small adsorption barrier,[4,5] adiabatic electronic structure calculations using density functional theory yield a potential energy surface with large purely attractive portions[6−8] so that the dissociation probability for all kinetic energies should be close to one.

Just recently, it has been shown that spin selection rules could play an important role in understanding the dissociation dynamics of O_2/Al(111).[9,10] Upon adsorption, oxygen changes its spin state from the gas-phase triplet state to the singlet state. Because of the low density of states of aluminum at the Fermi level, the probability for the triplet-to-singlet transition is rather small. Hence, the O_2 molecules do not follow the adiabatic potential energy curve but stay in the triplet state, which becomes repulsive close to the surface according to electronic structure calculations using density functional theory (DFT) within the generalized gradient approximation (GGA).[11,12]

However, the description of the oxygen molecule using GGA functionals is problematic. For example, the binding energy of O_2 is overestimated by more than 0.5 eV using some of the most popular GGA functionals.[9,12,13] Hence, it would be desirable to treat the O_2/Al(111) system with a more accurate method. Unfortunately, the description of metal surfaces requires the use of the slab approach within the periodic supercell concept in order to reproduce the delocalized nature of the metal orbitals, and this prohibits the use of accurate wave-function-based ab initio methods.

Still, for metal clusters a comparison between DFT and wave-function-based quantum chemistry methods is possible. In fact, the interaction of molecules with small metal clusters is interesting in its own right[14] because metal clusters can exhibit properties that are distinctly different from those of atoms or bulk materials. In fact, heterogeneous reactions occur differently on metal clusters than on bulk surfaces.[15] The area of metal cluster chemistry is currently very active, prompted in part by the development of methods for producing these species in the gas phase, both neutral and charged.

As far as aluminum clusters are concerned, oxidation reactions have indeed intensively been studied experimentally[15−19] because of the technological importance of this process. Experiments indicate that the reaction of O_2 with small aluminum cluster ions is activated with barriers larger than 0.1 eV.[15,16]

Theoretical studies have been performed for small Al_n[20−22] and Al_nO_m[23] clusters. Recently, neutral, cationic, and anionic Al_n and Al_nO clusters with $n = 2-10$ have been studied systematically[24] within DFT using the B3LYP functional. According to DFT and Hartree−Fock calculations, Al_4 and Al_5 clusters prefer a planar structure.[22,24] The stable planar structure of Al_4 is a rhombus with occupied ring-like σ bonding states and unoccupied π bonding states. In fact, the recent finding of aromatic character in Al_4^{2-} clusters has expanded the aromaticity

* Corresponding authors. E-mail: axel.gross@uni-ulm.de; mavridis@chem.uoa.gr.
[†] Ulm University.
[‡] National and Kapodistrian University of Athens.
[§] National Hellenic Research Foundation.

10.1021/jp711991b CCC: $40.75
Published on Web 04/05/2008

concept into all-metal complexes.[25,26] The structures of larger nonplanar Al clusters differ from those of crystals.[22,24]

Interestingly enough, in a recent combined experimental and theoretical study[27] the importance of spin selection rules was also demonstrated for O_2 interacting with small Al anion clusters (~10 to 20 atoms) leading to an odd/even pattern in the reactivity with O_2 as a function of the number *n* of atoms in the Al clusters.

Still, the calculations have all focused on the equilibrium structures of pure and oxidized Al clusters. The potential energy surface of oxygen interacting with Al clusters has, to the best of our knowledge, hardly been mapped out yet by first-principles electronic structure methods. DFT calculations found a barrier of 0.2 eV for the reaction of O_2 with octahedral-like Al_6 cluster in the spin triplet state.[28] The dynamics of the oxidation of aluminum nanoclusters with more than 200 000 Al atoms has been studied by molecular dynamics simulations,[29] but in this case an empirical interaction potential between dioxygen and aluminum had been used. Hence, it is not clear whether oxygen atoms can spontaneously dissociate on small Al clusters, or whether the dissociation corresponds to an activated process.

We have addressed the pathways for oxygen dissociation at small Al clusters using both density functional theory and wave-function-based quantum chemistry methods. In addition, we have compared the slab and cluster approach in modeling the O_2 adsorption on the Al(111) substrate within DFT. Although we confirm the previous adiabatic periodic DFT results, all of the cluster calculations find a non-vanishing barrier in the O_2 adsorption as long as either accurate wave-function-based quantum chemistry methods or hybrid DFT functionals with a certain fraction of Fock exchange are used. However, because the employed cluster models are still too small to give an appropriate representation of the Al(111) surface, we cannot discern whether these differences are due to the improvement of the exchange-correlation treatment in the cluster calculations or whether they just are caused by the different O_2−Al interactions in clusters and extended surfaces. Still, these results demonstrate that correlation effects are important for the determination of the adsorption barrier in the system O_2/Al and that they require further attention, from both a computational as well as a fundamental point of view.

II. Theoretical Methods

The electronic structure calculations have been performed with both quantum chemistry codes[30,31] as well as with a periodic DFT program, the *VASP* code.[32] The quantum chemical calculations for the finite molecular systems were carried out using both the *MOLPRO*[30] and *GAUSSIAN* packages.[31] The calculations presented in the next section have been obtained using *MOLPRO* and the correlation consistent basis sets cc-pVTZ for Al (15s9p2d1f) and aug-cc-pVTZ for O (11s6p3d2f), both generally contracted to $[5s4p2d1f/_{Al}\ 5s4p3d2f/_{O}] \equiv TZ$.[33] For the largest molecular system studied, Al_4O_2, the total one-electron space comprises 228 spherical Gaussians. The chemical species examined in the present work are $O_2(X^3\Sigma_g^-)$, $Al_2(X^3\Sigma_g^-)$, and $Al_4(^1A_1)$, but we were focused mainly on the interaction of $Al_4 + O_2$. All calculations were done at the complete active space self-consistent field (CASSCF) + single + double replacement level (CASSCF + 1 + 2 = MRCI). The Davidson correction (+Q) for unlinked quadruples was also employed to ameliorate size non-extensivity errors. The multireference approach was deemed as necessary for the description of the Al_4−O_2 potential energy surface (PES). No core or relativistic effects or further corrections have been taken into account in the present work because they are considered of limited importance for the description of the O_2 + Al system.

III. Results

We will first describe the results of quantum chemical calculations addressing the interaction of small Al clusters with O_2 and then extend these calculations to larger Al clusters using density functional theory. Although the cluster calculations are certainly motivated by the experiments for the O_2/Al(111) system, these calculations are certainly interesting in their own right, again, even if the chosen cluster structures are motivated by surface structures.

A. Interaction of O_2 with Planar Al_4 Clusters: A Wave-Function-Based ab Initio Approach. First we address the interaction of oxygen with a square-planar Al_4 cluster that could serve as a very simple model for an Al(100) surface, and a rhombus- or diamond-shaped planar Al_4 cluster as a model for the Al(111) surface. In order to validate our calculations, we have first studied the O_2 and Al_2 dimers and compared the results with experimental values. Our findings on O_2 and Al_2 indicate the adequacy of both the basis sets as well as the methods used for the purposes of the present work. The bonding of the $X^3\Sigma_g^-$ state of O_2 is described by the valence-bond-Lewis (vbL) diagram (1).

The experimental bond distance (r_e) and the dissociation

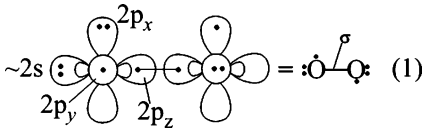

$$O(^3P;\ M_L = \pm 1)\ O(^3P;\ M_L = \mp 1)\ X^3\Sigma_g^-$$

energy (D_e) are r_e = 1.208 and D_e = 120.2 kcal/mol (=5.21 eV).[34] At the MRCI(+Q)/TZ level, the corresponding values are r_e = 1.213 (1.216) Å and D_e = 113.0 (115.3) kcal/mol (= 4.90 (5.00) eV), in relatively good agreement with experiment. The binding in the X state of the Al_2 dimer is more involved; as shown in the vbL diagram (2), the two Al atoms are held together by two (1/2)π (one electron) bonds.

Scheme 2 is corroborated nicely by the CASSCF Mulliken

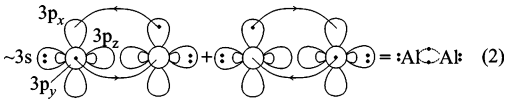

$$Al(^2P;\ M_L = \pm 1)\ Al(^2P;\ M_L = \mp 1)\ X^3\Sigma_g^-$$

atomic populations: $3s^{1.70}3p_z^{0.25}3p_x^{0.49}(3d)^{0.06}$. At the MRCI-(+Q)/TZ level, we obtain for the dimer bond length r_e = 2.500 (2.500) Å and for the binding energy D_e = 31.1 (30.9) kcal/mol (= 1.35 (1.34) eV), respectively, in fair agreement with the experiment (r_e = 2.466 Å, D_e = 35.2 kcal/mol (= 1.53 eV))[34] considering the level of calculation.

It should be mentioned at this point that our reference wave function (CASSCF) for O_2 was constructed by allotting eight "valence" ($2p^4$) electrons in six orbitals. In Al_2, six active electrons (two 3s plus one 3p electron on each Al atom) were distributed in eight orbitals. Out of these reference spaces, single and double excitations (including the $2s^2$ electrons omitted in the CASSCF description of O_2), resulted in the internally contracted MRCI wave functions[30] of O_2 and Al_2. All calculations were performed under C_{2v} symmetry constraints.

We turn now to the electronic structure and geometry of the Al_4 cluster. Certainly, there are many ways that one can

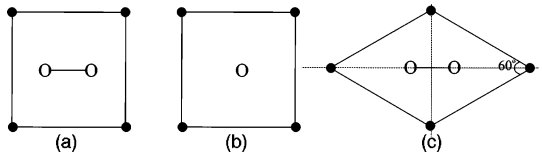

Figure 1. Top view of the planar Al_4 clusters together with the O_2 geometry considered in the multireference calculations. (a) Parallel and (b) perpendicular attack (along the C_4 axis) of O_2 at the square-planar cluster, (c) parallel attack at the rhombus-shaped cluster.

geometrically arrange four Al atoms in space, singlets, triplets, or quintets (see also the DFT results of refs 35 and 36 on the structure of Al_4). Our purpose is to "simulate" the Al−metallic surface with four Al atoms, followed by its interaction with the $X^3\Sigma_g^-$ state of O_2. The Al_4 geometrical arrangements that we have considered are the square-planar (D_{4h}) and the 60°-rhombus (D_{2h}) as simple models for Al(100) and Al(111) surfaces, respectively. A top view of these clusters together with the geometry of the approaching O_2 molecule is shown in Figure 1.

For the square Al_4 geometry, CASSCF functions constructed by distributing the 12 valence (active) electrons of the four Al-($3s^2 3p^1$;^{2}P) atoms in 10 orbitals [CASSCF(12/10)], indicate that the (open) singlet of the square-planar arrangement ($^1A_1$) is lower in energy than the high-spin $^5A_1$ state by about 31 mE_h (= 19.5 kcal/mol = 0.85 eV). From the corresponding tetrahedral (T_d) singlet, the $^1A_1$ state is lower by 9 mE_h and practically degenerate with the high-spin T_d structure. At the previously described CASSCF/TZ level of theory, the $^1A_1$ (D_{4h}) Al_4 structure is consistent with the following diagram:

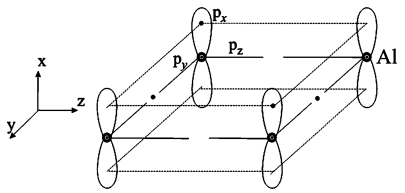

(3)

The bonding structure (3) is also corroborated by the Mulliken atomic populations, $3s^{1.59}3p_z^{0.30}3p_x^{0.55}3p_y^{0.46}(3d)^{0.09}$. Note that the attractive interaction comprises a two electron-four center ($2e^-$-4c) σ delocalized bond (on the yz plane), and a $2e^-$-4c π_x delocalized bond (yz being the nodal plane), reminding of a $2e^-$ "aromatic" system. At this level of theory, CASSCF(12/10), the optimized Al−Al bond distance is 2.626 Å and the atomization energy AE = 53.9 kcal/mol (= 2.34 eV), or 53.9/4 = 13.5 kcal/mol (= 0.59 eV) per Al−Al bond. These numbers should be contrasted with the corresponding CASSCF(6/8) values of Al_2 ($X^3\Sigma_g^-$), namely, r_e = 2.528 Å and D_e = 28.5 kcal/mol (= 1.24 eV). Going to a full valence CASSCF calculation on Al_4, that is, 12 electrons in 16 orbitals [(one 3s + three 3p) × 4], our $^1A_1$ (open singlet) wave function contains 1 774 000 configuration state functions (CSFs) and a total energy $E(^1A_1)$/[CASSCF(12/16)] = −967.75253 E_h, 94.5 mE_h (= 59.3 kcal/mol = 2.57 eV) lower than the $E(^1A_1)$/[CASSCF(12/10)] total energy. At the CASSCF(12/16) level, the Al−Al bond distance is 2.656 Å, similar to the 12/10 result, but the atomization energy AE = 112.2 kcal/mol (= 4.87 eV), or the per Al−Al bond strength, 112.2/4 = 28.0 kcal/mol (= 1.22 eV), is almost identical to the corresponding CASSCF(6/8) D_e value of $Al_2(X^3\Sigma_g^-)$, 28.5 kcal/mol (= 1.24 eV).

Our purpose is to study the interaction of $Al_4 + O_2$, and it is understandable that valence MRCI (CASSCF + 1 + 2) calculations are not feasible at a complete CASSCF level (24 electrons in 24 orbital functions). In the light of the above, the square $Al_4(^1A_1) + O_2$ surface has been studied at the MRCI level with a reference CASSCF wave function constructed by allotting 20 electrons (12 from Al_4 + 8 from O_2) in 12 orbitals. This kind of calculation allows for a smooth stretching (dissociation) of the $O_2(X^3\Sigma_g^-)$ molecule and a fair description of $Al_4(^1A_1)$. Even at this level, we were obliged to truncate the CASSCF(20/12) CSFs in order to perform the subsequent MRCI computations. A threshold of 0.01 was imposed resulting to MRCI expansions ranging from 2×10^6 to 3×10^6 internally contracted CSFs.

As was mentioned in the previous section, we performed CASSCF(20/12) + 1 + 2 calculations on the $Al_4(^1A_1) + O_2(X^3\Sigma_g^-)$ system. Two attack paths were chosen: (a) The intermolecular axis of O_2 being parallel to the square-planar configuration of Al_4 and (b) the O_2 intermolecular axis being perpendicular to the plane of Al_4 atoms, that is, coinciding with the C_4 axis of Al_4 (see Figure 1a and 1b, respectively). All calculations were done under C_{2v} constraints. In both attacks, a and b, the Al−Al bond length was first kept constant at 2.67 Å changing only the R and r_{OO} distances, R being the O_2 center of mass distance from the Al_4 plane and r_{OO} the O−O distance.

The PES at the MRCI+Q/TZ level of the approach illustrated in Figure 1a is displayed in Figure 2. At this level, a global minimum is observed at about R = 1.33 Å, r_{OO} = 1.50 Å, and a total energy of −1118.124 E_h. At this point, a re-optimization of R, r_{OO}, and r_{AlAl} distances at the MRCI [CASSCF(20/12) + 1 + 2] level of theory gave R = 1.16 Å, r_{OO} = 1.44 Å, and r_{AlAl} = 2.84 Å. An MRCI(+Q) calculation at this geometry gave a total energy of −1118.0052 (−1118.1299) E_h and a binding energy with respect to the super molecule $Al_4(^1A_1) + O_2(X^3\Sigma_g^-)$ of 103.3 (107.7) kcal/mol (= 4.48 (4.67) eV). Clearly, the O_2 molecule in its ground state binds strongly to the Al_4 square-planar (open $^1A_1$) configuration, with a synchronous charge transfer of about 0.6 e^- from Al_4 to O_2 and a concomitant significant lengthening of the r_{OO} bond distance by 0.23 Å with respect to its equilibrium value at infinity. The CASSCF(20/12) Mulliken atomic distributions of the $Al_4(^1A_1)-O_2(X^3\Sigma_g^-) \equiv {}^3A_1$ complex are

$$3s^{1.82}3p_z^{0.39}3p_x^{0.19}3p_y^{0.32}(3d)^{0.09}|_{Al}$$

$$2s^{1.77}2p_z^{0.99}2p_x^{1.80}2p_y^{1.70}(3d)^{0.06}|_{O}$$

Note the corresponding populations of $Al_4(^1A_1)$ and $O_2(X^3\Sigma_g^-)$ at infinite separation at the CASSCF(12/10) and CASSCF(8/6) levels, respectively:

$$3s^{1.59}3p_z^{0.30}3p_x^{0.55}3p_y^{0.46}(3d)^{0.09}|_{Al}$$

$$2s^{1.97}2p_z^{1.02}2p_x^{1.48}2p_y^{1.48}(3d)^{0.04}|_{O}$$

Note that on the $\sigma(yz)$ plane the $3s3p_z3p_y$ populations on Al before and after the interaction remain practically constant, 2.35 and 2.53 e^-, respectively; the same holds true for the O_2 molecule: 4.47 and 4.46 e^-. It is expected, according to diagrams 1, 3, and Figure 1a, that the bonding interaction takes place along the x axis or the $\pi_x(yz)$ plane of Al_4. Indeed, this plane feeds electrons to the $2p_x$ orbital of each oxygen atom of O_2, which is enriched at the equilibrium by a total of 0.6 electrons. As a result, its bond length increases by 0.23 Å. We recall that the experimental bond length difference between $O_2^-(X^2\Pi_g)$ and $O_2(X^3\Sigma_g^-)$ is 0.14 Å.[34]

Our conclusion is that a "dissociative" adsorption is simulated along the parallel attack (Figure 1a) along the triplet PES. Figure

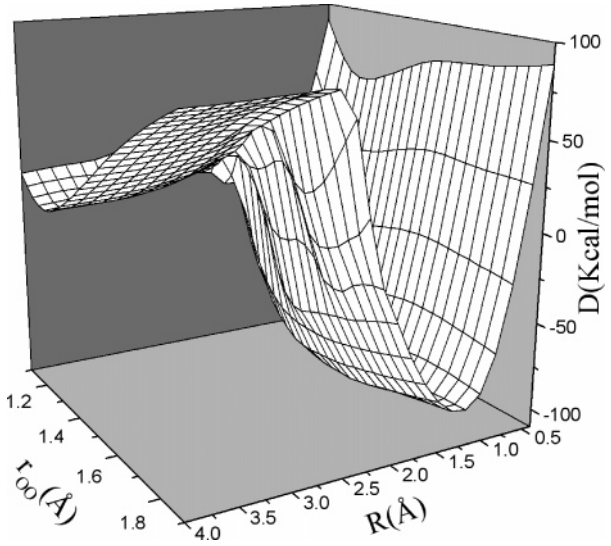

Figure 2. $^3A_1$ potential energy surface of the $Al_4(^1A_1) + O_2(X^3\Sigma_g^-)$ parallel approach (square Al_4 cluster) at the MRCI+Q/TZ level of theory. The r_{Al-Al} distance is kept fixed at 2.67 Å.

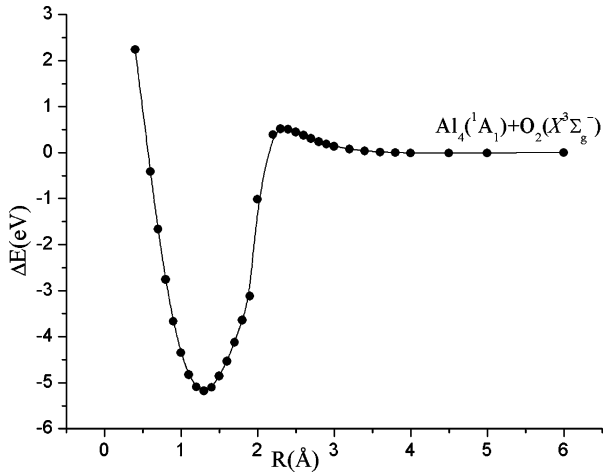

Figure 3. $^3A_1$ potential energy profile of the O_2/Al_4 PES (see Figure 2) in eV for a fixed O−O distance of $r_{OO} = 1.40$ Å as a function of the distance R of the O_2 molecule from the Al_4 plane.

3 shows a potential energy profile at $r_{OO} = 1.40$ Å. An energy barrier is observed at $R = 2.2$ Å close to 13 kcal/mol (= 0.56 eV), which can also be discerned in the PES of Figure 2.

We describe now the "perpendicular" attack; see Figure 1b. According to our previous analysis, a strong π_x^2 (*yz* nodal plane) $Al_4-O_2(2p_y^1 2p_z^1)$ interaction is expected. In this approach, the σ O−O bond is along the *x* (C_4) axis. According to diagram 4 and by symmetry, the O_2 equilibrium position should be with its center of mass in the Al_4 square plane with the one oxygen atom above and the other below the nodal *yz* plane.

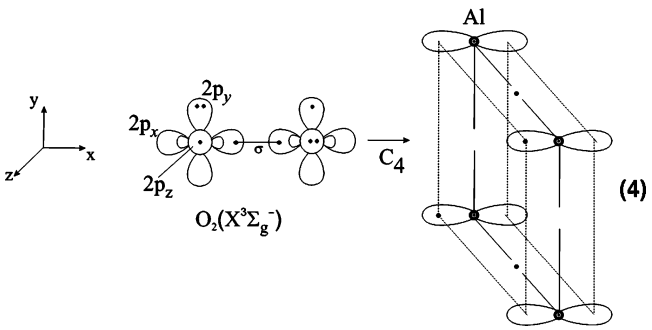

(4)

This is exactly what happens at the MRCI[CASSCF(20/12) + 1 + 2](+Q) level. Our CASSCF Mulliken atomic populations are quite revealing:

$$3s^{1.82}3p_z^{0.34}3p_x^{0.06}3p_y^{0.34}(3d)^{0.12}|_{Al}$$

$$2s^{1.81}2p_z^{1.71}2p_x^{1.36}2p_y^{1.71}(3d)^{0.06}|_{O}$$

Observe that although the Al $3s3p_z3p_y$ populations (2.50 e^-) are identical to that of the parallel attack (2.53 e^-), the $3p_x$ orbital of each Al atom transfers 0.5 e^- to the $2p_y$,$2p_z$ orbitals of each O atom of O_2; the sum of 2s and $2p_x$ populations is close to 3 e^- as it should be. In other words, a total of about 1.2 e^- migrates from Al_4 to O_2, leading to the ionic system $Al_4^+ O_2^-$. Optimizing the geometry of the Al_4-O_2 complex at the MRCI-(+Q) level of theory while maintaining the D_{4h} constraints, we obtain the following equilibrium geometry: $R = 0.0$ Å, $r_{OO} =$ 2.024 (2.046) Å, and $r_{AlAl} = 2.673(2.69)$ Å. Note that the O−O bond has been practically broken. At the same level of theory, the binding energy is 158.3 (160.7) kcal/mol (= 6.87 (6.97) eV) with respect to $Al_4 + O_2$. The MRCI(+Q) total energy of the $Al_4^+ O_2^-$ complex is −1118.0929 (−1118.214) E_h. The perpendicular attack of O_2 leads clearly to a dissociative "ionic adsorption" on the Al_4 cluster, with a binding energy considerably larger by 55 (53) kcal/mol (= 2.39 (2.30) eV) than that of the parallel attack.

The interaction of O_2 with the square-planar Al_4 can be regarded as a very simple model for the O_2/Al(100) system. In order to account for the O_2/Al(111) system, we also consider the parallel approach of $O_2(X^3\Sigma_g^-)$ to a planar 60° rhombus-like Al_4 configuration with the O_2 molecular axis parallel to the long diagonal axis of the rhombus (see Figure 1c). First, the Al−Al distance of the free Al_4 rhombus ($^1A_1$) was optimized at the CASSCF (12/16) level under the 60° angle constraint (point group D_{2h}). The r_{AlAl} equilibrium distance was found to be 2.605 Å, which is 0.051 Å shorter and the total energy about 9 mE_h lower ($E = -967.76119$ E_h) than the corresponding values of the square-planar Al_4 configuration.

Next, the equilibrium structure of the Al_4-O_2 complex was determined at the MRCI(20/12) level, under the geometry constraints dictated by the configuration shown in Figure 1c (point group symmetry C_{2v}; $^3A_2$). In other words, the varied parameters are r_{OO}, r_{AlAl}, and R (the distance between the centers of mass of the O_2 bond and the Al_4 rhombus), maintaining the angle of 60°. Our results are the following (in parenthesis, results of the square-planar parallel attack): $r_{OO} = 1.44(1.44)$ Å, r_{AlAl} = 2.78(2.84) Å, and $R = 1.38(1.16)$ Å. The main difference between the square-planar and the rhombus is the R distance, being significantly smaller in the former case, indicating the more open square-planar configuration of Al_4, which allows the O_2 molecule to come closer to the plane of the Al atoms. The total MRCI(+Q) energy $E(^3A_2) = -1117.9736$ (−1118.0978) E_h, is higher than the $^3A_1$ (square-planar) state by 32 (32) mE_h ≈ 20 kcal/mol (= 0.87 eV). This corresponds to a binding energy of the $^3A_2$ state $D_e = 77.2(80.9)$ kcal/mol (= 3.35 (3.51) eV), as compared to 103.3 (107.7) kcal/mol (= 4.48 (4.67) eV) of the $^3A_1$ square-planar configuration.

Figure 4 displays a potential energy profile through the $^3A_2$ surface, that is, total energy as a function of R with $r_{OO} = 1.40$ Å and $r_{AlAl} = 2.67$ Å. The morphology of the $^3A_1$ and $^3A_2$ profile curves is rather similar, as expected. The observed $^3A_2$ energy barrier at 2.9 Å amounts to 5.6 kcal/mol (= 0.24 eV) as contrasted to 2.2 Å and 13 kcal/mol (= 0.56 eV) in $^3A_1$. A final comment is in order. At infinity, the total minimized energy

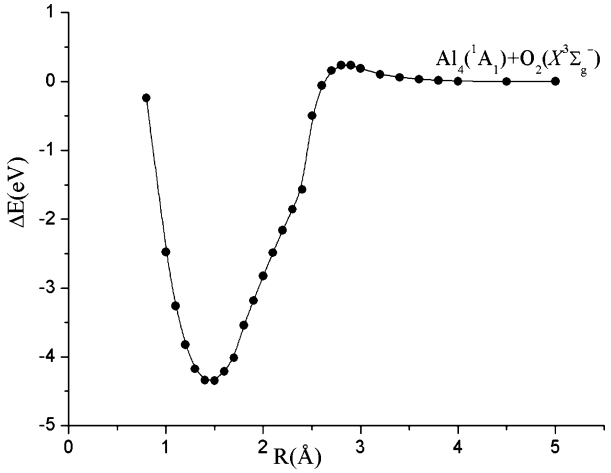

Figure 4. Potential energy profile in eV of the $^3A_2O_2/Al_4$ PES (Al_4 rhombus) for a fixed O−O distance of $r_{OO} = 1.40$ Å as a function of the distance R of the O_2 molecule from the Al_4 plane.

of the supermolecule $Al_4 + O_2$ of the $^3A_1$ surface at the MRCI-(20/12)(+Q) level is −1117.8519 (−1117.9694) E_h, about 11 (11) mE_h lower than the corresponding value of the $^3A_2$ surface. This is consistent with the −9 mE_h CASSCF(12/16)) energy difference between the rhombus and the square-plane Al_4 configuration reported before.

The discussion above is clearly in support that the mode of interaction between the rhombus and square-planar parallel O_2 attacks are of the same nature.

B. Large Al Clusters and the Al(111) Substrate: A DFT Approach. The results of the previous sections were obtained on a high level of accuracy concerning basis sets and the many-electron model. In essence, we have seen that there is a small barrier for adsorption of O_2 on Al_4, if one describes the interaction between O_2 and Al_4 on a level that lies beyond simple adiabatic DFT. One of the most important questions is still open: Is the calculated barrier present due to the finite size of the Al_4 cluster and its complicated orbital spin structure (see, e.g., ref 21), or is the determination of this barrier a real step toward correctly describing the adsorption process of O_2 on Al-(111)?

As a preliminary study, we performed DFT calculations using the PBE functional[11] to describe the exchange and correlation effects with the 6-311G(d) Gaussian basis set.[37] For these particular calculations, we employed an Al_4 60° rhombus with an Al−Al spacing of 2.86 Å as in the crystal lattice. Because the PBE functional does not always describe the dissociation limit correctly at all spin states, we consider three cases of the total spin of the whole system Al_4-O_2: singlet, triplet, and quintet. The energies are shown as contour diagrams in Figure 5 together with the adiabatic minimum energy, indicating possible changes of the total spin during the O_2 approach. Far away from the cluster, as expected, the preferred spin is triplet, due to the fact that the ground state of O_2 with a bond length of 1.25 Å is a triplet, the Al_4 cluster being in a singlet state. However, in all three spin cases the rhomboidal cluster can bind two oxygen atoms separated by 3.45, 3.72, and 3.60 Å in singlet, triplet, and quintet states, at heights 0.8, 0.9, and 0.9 Å from the rhomboidal plane, respectively, and with respective total energies of −1119.535, −1119.483, and −1119.413 E_h.

Keeping in mind that the Al−Al separation was held constant at 2.86 Å, the relatively large values of the O−O separation of the O atoms bound to the cluster clearly suggest an O_2 bond breaking. Given that the energy of the separated system O_2 + Al_4 rhombus is −1119.200 E_h and of the bound singlet system is −1119.535 E_h, we arrive at a O_2/Al_4 binding energy of 0.335 E_h (= 210 kcal/mol = 9.12 eV), which is much larger than the corresponding value obtained at the MRCI level. Furthermore, as seen from Figure 5, at this level of theory, in the vicinity of the Al_4-rhomboidal cluster there is no O_2 dissociation barrier, in accordance with relevant findings of ref 8 for the Al(111) surface, but at variance with the MRCI calculations just presented. It should be mentioned that at the place of the expected slight energy barrier the DFT-BPE calculations show convergence failures. However, the local environment considerations using just Al_4 clusters confirm the well-known fact that small clusters are not sufficient to resolve the problem of the experimentally suggested small adsorption barrier[4,5] and a more elaborate approach is needed.

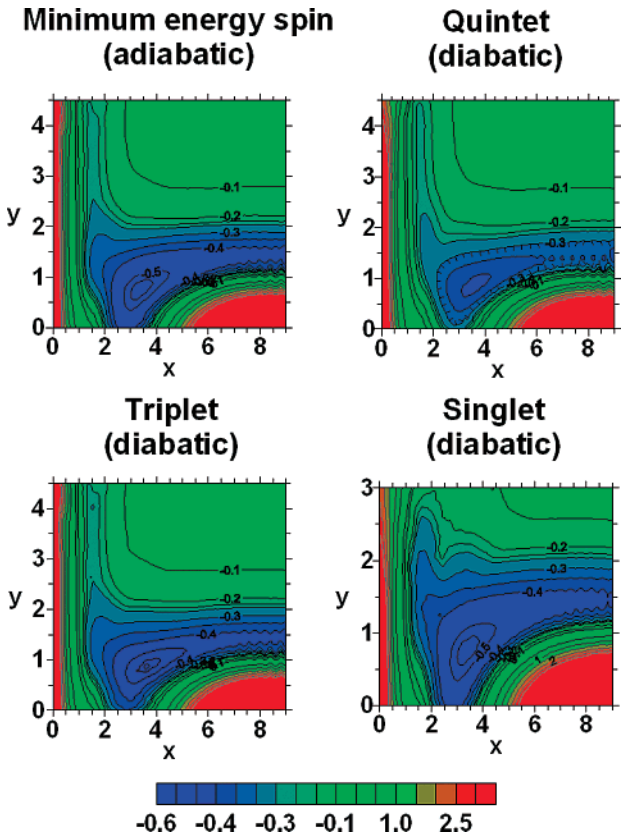

Figure 5. Diabatic singlet, triplet, quintet, and minimum energy adiabatic approach of O_2 perpendicularly to the Al_4 rhombus, with the O_2 axis parallel to the large diagonal Al(1)−Al(3). The horizontal x axis represents the O−O separation, and the vertical y axis represents the height of the O_2 center from the Al_4 rhombus center in Å. The color coding of the level spacing in E_h is given in the bottom panel of the figure.

In order to address the question of the O_2−Al interaction as a function of the cluster size in a systematic way, we employed a three-step approach taking into account that it is not possible to increase the cluster size in the calculations while keeping a high chemical accuracy. In a first step, we determined the size of the Al cluster that is sufficiently large enough to reproduce the slab calculations for Al(111) within the PBE functional[11] using a periodic plane-wave DFT code (*VASP*[32]). In the second step, we compared the cluster calculations obtained within the periodic DFT code with the equivalent calculations using a quantum chemistry program for finite systems (*GAUSSIAN*[31]). Finally, in the third step we increased the chemical accuracy again up to a level that is still feasible by using hybrid DFT functionals.[38,39]

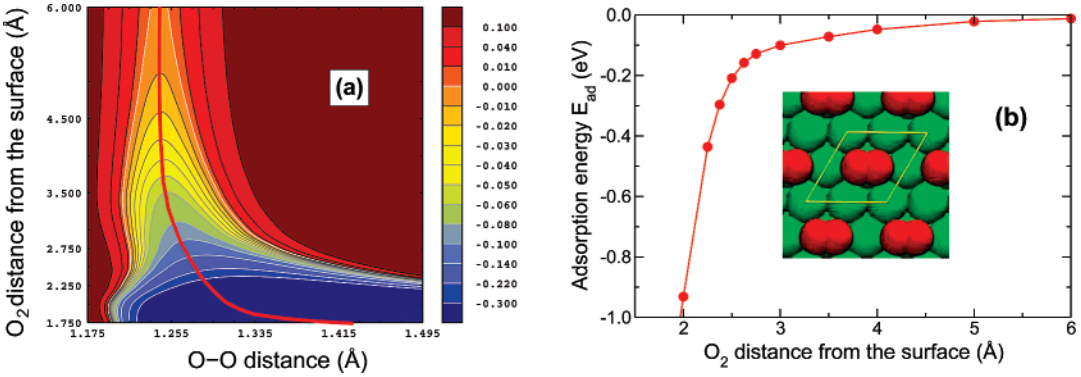

Figure 6. Calculated potential energy of O_2 above the on-top site of Al(111) in a bridge-top-bridge configuration: (a) Two-dimensional elbow plot as a function of the O−O distance and the O_2 center of mass distance from the surface. The level heights in eV are indicated at the right-hand side. (b) Potential energy curve along the minimum energy path indicated in a. The inset illustrates the O_2 configuration and the surface unit cell.

We particularly focus on the configuration with the center of mass of the O_2 molecule located above an Al atom of the Al(111) surface and the molecule oriented parallel to the surface in a so-called bridge-top-bridge (btb) configuration, which means that the O_2 center of mass is located above an Al top site while the two oxygen atoms are located in lateral directions pointing toward the Al bridge sites. In addition, we include a hollow-bridge-hollow (hbh) like configuration with the molecule oriented parallel to the surface as in Figure 1c, that ensures the comparability with the corresponding quantum chemistry calculations of the previous section.

The periodic surface calculations were done using (2×2) and (3×3) hexagonal unit cells with a lattice constant of 4.04 Å corresponding to a Al−Al distance of 2.86 Å, 7 layers of Al(111) slab, and 14 Å vacuum above the metal surface. There was one O_2 molecule per surface unit cell with orientation bridge-top-bridge or hollow-bridge-hollow parallel to the surface. The ionic cores were represented by projector augmented wave (PAW) potentials[40] as constructed by Kresse and Joubert.[41] The results were obtained for an energy cutoff of 350 eV and $7 \times 7 \times 1$ k points ($5 \times 5 \times 1$ for the (3×3) cell). A Methfessel−Paxton and Gaussian smearing of $\sigma = 0.1$ eV was applied and the results were extrapolated to $\sigma \rightarrow 0$ eV. The Al(111) slab was kept fixed at the positions of the relaxed clean surface.

The corresponding clusters were obtained by cutting them out of the fixed clean surface without any further relaxation (if not mentioned otherwise). Five different clusters were created: Al_4 in tetrahedron shape, Al_4 in rhombus or diamond shape, Al_{13}, Al_{22}, and Al_{41}. The cluster calculations with *VASP* were done in a supercell of dimensions $14 \times 14 \times 20$ Å^3 for the Al_4 clusters and up to $16 \times 18 \times 20$ Å^3 for the Al_{41} cluster. The periodic images of the clusters are separated enough to be noninteracting. Hence, the integral over the first Brillouin zone can be replaced by a single k-point calculation done at the Γ point, the origin of the reciprocal space. The final calculations with *GAUSSIAN* were done with the B3LYP functional and the 6-31G* basis.

Because we intended to describe an unpolarized Al(111) surface by cluster models, we assumed zero initial magnetization of the Al atoms. Note that in periodic calculations the total spin of the system is not a conserved quantity. In most cases, the final magnetization of the clusters remained zero; however, the Al_4 clusters behaved completely differently: magnetization 4 μ_B turned out to be the ground state of the diamond-shaped Al_4 cluster with a nearest-neighbor distance of 2.86 Å (the distance of the Al-surface atoms) corresponding to a quintet state, while magnetization 2 μ_B (triplet state) is the ground state of the same cluster when all atoms are allowed to relax to distances of 2.60 Å. Note that we found a singlet state to be the electronic ground state at the CASSCF level for this Al−Al spacing (see the previous section). The tetrahethron-shaped Al_4 cluster always prefers magnetization 4 μ_B (quintet state) in its ground state. Therefore, the Al_4 clusters were calculated with an initial magnetization of 4 μ_B. All other larger Al clusters were calculated with an initial magnetization of 0 μ_B (singlet state), which they usually kept during the electronic iterations. In some cases, this had to be stabilized by increasing the smearing to 0.5 eV (see text below).

For selected configurations, we have determined the whole two-dimensional potential energy surface as a function of the O_2 center of mass distance from the surface and the O−O distance within a (2×2) surface unit cell (see Figure 6a). However, we will focus mainly on the minimum energy path along this two-dimensional cut through the potential energy surface, which is indicated as the red line in Figure 6a. The corresponding potential energy curve is plotted in Figure 6b. The energy zero refers to O_2 in the gas phase. We will in fact use the same O−O distances as a function of the O_2 distance from the surface in all subsequent cluster calculations. Thus, most of the following plots will show the O_2 minimum energy path and in addition the O_2 magnetization in dependence of the height of O_2 above the Al surface or Al cluster, respectively.

Previous DFT calculations[9,10] have shown that the crucial region for the existence of a barrier is about 2.5 Å above the surface. When the O_2 molecule has crossed this point, it dissociates and the O atoms become strongly bound to the Al surface. Then the minimum energy path of the adsorption energy drops down to large negative values for distances smaller than 2 Å above the surface. Because we are here concerned mainly with the possible existence of an adsorption barrier, we will focus on potential curves for distances larger than 2.0 Å from the surface.

As far as the dependence of the O_2/Al(111) interaction on the slab thickness in the periodic DFT calculations is concerned, we found that the O_2/Al(111) interaction energy changes by up to 20 meV when the slab thickness is increased from 5−7 layers. In contrast, there are hardly any changes if the number of layers is further increased. This is also reflected in the dependence of the work function on the layer thickness (see Table 1). Hence, all further slab calculations were done with 7 layers.

For the cluster calculations using the *VASP* code, we encoutered several problems. Although they are mainly of technical character, we will still discuss them here because this will shed some light on the electronic structure of both the oxygen molecule and the Al clusters. In contrast to the Al

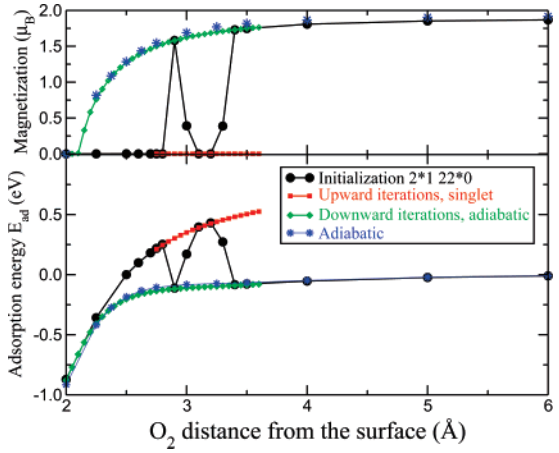

Figure 7. Calculated O_2 magnetization in μ_B and adsorption energy E_{ad} in eV of O_2 in a bridge-top-bridge geometry above the Al_{22} cluster as a function of the O_2 distance from the surface in the singlet and adiabatic ground state for different wave function initializations (see text).

TABLE 1: Calculated Work Function of Al(111) as a Function of the Slab Thickness in the Supercell Calculations

no. of layers	work function (eV)
3	3.85
5	4.12
7	4.04
9	4.06
11	4.06

surface, which has a very simple magnetic structure, namely zero magnetization, the different Al clusters show a multitude of different magnetization configurations each with its own local energetic minimum, as already found for the planar Al_4 clusters at the MRCI level (see above). The complicated spin structure of small- to medium-sized metal clusters is a well-known fact[42] and was studied for small Al clusters before (see, e.g., ref 24).

To overcome this problem, we initialized the magnetization of all Al atoms to be zero (exception Al_4), while initializing the magnetization of O_2 to the triplet state (2 μ_B). This did still not lead to well-converged results. Even without O_2, the Al clusters converge seemingly randomly into different spin states depending on the random wave function initialization. The corresponding energies also differ by up to several electronvolts. Thus, as an additional measure we chose a smearing temperature of 0.5 eV, which kept the Al cluster in a nonmagnetic ground state. Such a smearing is rather high but still acceptable because the energetics of the O_2/Al interaction remains basically the same when the smearing in increased from 0.1 to 0.5 eV.

Using this scheme, all larger aluminum clusters finally remained at zero magnetization, as they should. However, performing a straightforward determination of the minimum energy path of O_2 interacting with Al_{22} leads again to some seemingly erratic results, which is illustrated by the circles in Figure 7: The energy and accordingly the magnetization jump up and down when the molecule approaches the cluster. In order to determine the nature of the jumps, we performed careful calculations in which we changed the O_2 distance from the surface in rather small steps using the converged charge density and wave function of the last height step for the next one. Moving upward away from the surface (boxes in Figure 7), the molecule remained nonmagnetic; that is, it stayed in the singlet state. Alternatively, if one moves in small steps downward to the surface starting with the triplet state (diamonds in Figure 7), then the curves remain smooth and the state changes

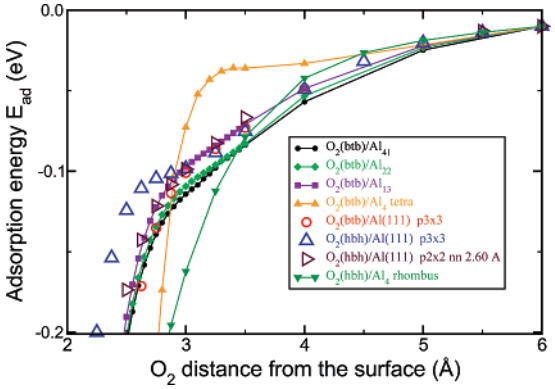

Figure 8. Comparison of the minimum energy path of O_2 interacting with different Al clusters and a seven-layer Al(111) with different coverages and Al−Al distances. All results were obtained with the PBE functional.

adiabatically to the singlet state near the surface. This shows that the jumps that occurred in the straightforward calculations correspond to transitions between the singlet and the ground state. It further demonstrates the importance of an appropriate preparation of the initial state in the self-consistency cycles of the DFT calculation. With this approach, we were able to reliably reproduce the adiabatic ground-state curve as shown in Figure 7.

Having gained control over the ground state of the O_2/Al systems, we are in a position to compare the adiabatic minimum energy path for different cluster sizes with the corresponding results for the slabs using in all cases the PBE functional (Figure 8). First of all, we note that the two Al_4 clusters that we consider here (tetragonal and planar rhombus) exhibit characteristics that differ from the larger clusters and the slabs: Far away from Al, the interaction energies lie above the other curves due to lesser remaining density in the vaccuum but then suddenly drop below the other curves because of the strong interaction between the triplet O_2 with magnetization 2 μ_B and the Al_4 quintet. Despite these differences, all curves still decrease monotonically toward the surface exhibiting no barrier for O_2 adsorption. Hence, one can conclude that the PBE functional does not produce any activated behavior in the O_2/Al interaction, as already found in our preliminary DFT calculations reported above (see Figure 5).

The results for the larger cluster are in a rather good agreement with those for the slab calculations. Already for an Al_{22} cluster, slab and cluster results are almost on top of each other. One of the reasons might be that the larger clusters do not show any magnetization any more. The Al_{13} cluster still has a complex spin structure, but already the Al_{22} has a magnetization of nearly zero.

Because the Al_{22} cluster tends to have a low magnetization, this cluster seems to be a good compromise between speed and reproduction of the surface behavior in the range between 2.5 and 4 Å above the surface. Therefore, we have used this cluster in order to address the influence of adding Fock exchange to the functional, which requires the use of a quantum chemistry code for finite systems within a local basis set. Note that there are implementations within periodic DFT codes that allow us to use hybrid exchange/DFT functionals;[43] however, their computational effort is still too large to allow for the determination of a molecule−surface interaction PES.

Figure 9 shows the magnetization and the adsorption energy of O_2 approaching Al_{22} in a btb geometry obtained with both the *VASP* as well as the *GAUSSIAN* code using PBE-GGA. As in the periodic calculations, in the calculations for the finite

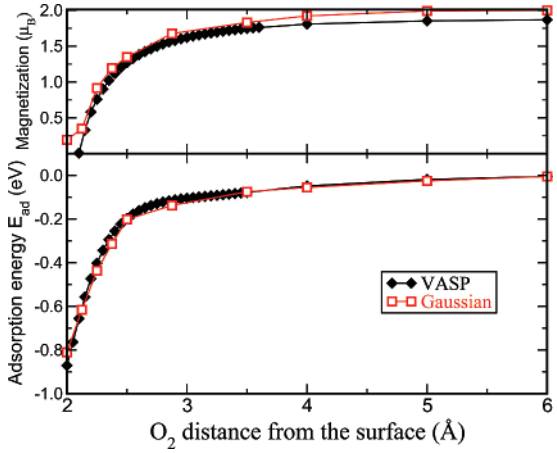

Figure 9. Comparison of *Gaussian* and *VASP* results for the O_2 magnetization in μ_B and the adsorption energy E_{ad} in eV of O_2 in a bridge-top-bridge geometry above the Al_{22} cluster.

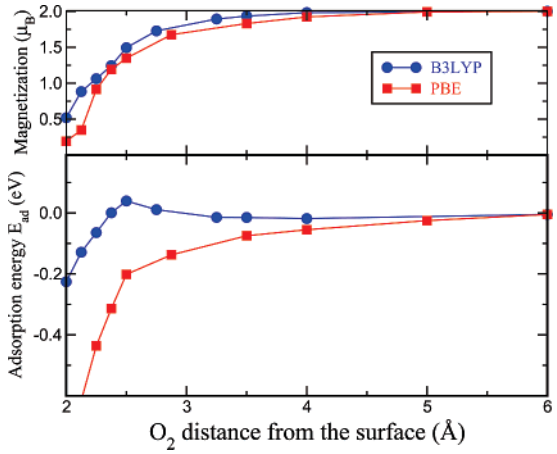

Figure 10. Comparison of DFT-B3LYP and DFT-PBE results for the O_2 magnetization in μ_B and the adsorption energy E_{ad} in eV of O_2 in a bridge-top-bridge geometry above the Al_{22}.

system within a localized basis set there are also severe problems finding the true local minimum for the Al cluster. The problem is even harder in localized codes if there is little control over the magnetic initialization of the calculation. Therefore, we pursued the following strategy: We started a calculation many times with the same configuration always choosing a different random initialization for the Al cluster. Then we ignored all results that did not converge at all or that were apparently not converged to the electronic ground state, indicated by erroneously large energies or large magnetizations. The plotted *GAUSSIAN* curve in Figure 8 is assembled of points with the lowest energy and very low magnetization on the Al atoms of the cluster. As Figure 9 demonstrates, the *GAUSSIAN* and *VASP* results agree to within 50 meV, which means that they are indistinguishable within the accuracy of the calculations.

Finally, we compare in Figure 10 PBE calculations with B3LYP calculations using the *GAUSSIAN* code. The B3LYP functional was chosen because it is the standard hybrid functional including Fock exchange used in DFT calculations for molecules, which successfully predicts a wide range of molecular properties. Also here, the strategy just described was used in order to cope with the convergence problems. Interestingly enough, the B3LYP adsorption energy curve stays substantially above the PBE curve and does in fact produce a barrier that is reminiscent of the barriers found in the multireference calculations reported in the first part of this paper.

IV. Concluding Remarks

We will first again summarize the current status of our understanding of the adsorption of dioxygen on Al(111). Molecular beam results suggest that the dissociative adsorption of O_2 on Al(111) corresponds to an activated process that is hindered by a small barrier.[4] Electronically adiabatic periodic DFT calculations, however, found that the dissociation of O_2 on Al(111) is not hindered by any barrier; that is, the adsorption should occur spontaneously,[6−8] in contrast to the experiment. Recently, it was shown that the low sticking probability for thermal O_2 molecules impinging on Al(111) can be related to spin selection rules that hinder transitions from the initial O_2 gas-phase triplet state to the singlet state upon adsorption.[9,10] A constrained DFT approach was employed to compute potential energy surfaces of O_2/Al(111) in different spin configurations, and the experimental sticking probability was qualitatively reproduced when restricting the O_2 molecule to motion on the spin-triplet PES only.

However, it would not be necessary to invoke any spin-selection rules in the dissociative adsorption of O_2 on Al(111) if there is a non-vanishing minimum adsorption barrier in the electronic ground state. Given the DFT slab results for the O_2/Al(111) system, this assumption would imply that current exchange-correlation functionals employed in periodic DFT calculations apparently fail to give a correct description of the adiabatic ground-state potential for O_2 approaching Al(111). Our calculations of O_2 impinging on planar Al_4 clusters using high-quality wave-function-based quantum chemistry methods clearly indicate the existence of such a minimum barrier, at least on planar Al_4 clusters.

Our DFT cluster and slab calculations using the PBE functional do not find any minimum barrier, irrespective of the cluster size and the surface unit cell, respectively. However, using a hybrid functional that contains a certain fraction of Fock exchange, we find a non-vanishing minimum barrier for the dissociative adsorption of O_2 on an Al_{22} cluster. Recently, a hybrid QM/QM scheme was proposed that takes advantage of the fact that errors of exchange-correlation functionals are rather short-ranged.[44−47] According to this method, exchange-correlation corrections can be evaluated using a properly chosen cluster representing a local section of the extended system. Applying this scheme, our results would indicate that slab calculations including Fock exchange should produce a minimum adsorption barrier. Thus the absence of a minimum barrier in the dissociative adsorption of O_2 on Al(111) in DFT slab calculations could indeed be an artifact of the improper description of many-body effects in the employed GGA-DFT functionals. Note that present-day DFT functionals seem to overestimate the interaction of the lowest unoccupied molecular orbital (LUMO) with metal substrates, as was shown recently.[48] This can lead to an unrealistically large downshift and occupation of the LUMO and could thus explain the absence of the barrier in the DFT calculations.

Now it is certainly not appropriate to naively extend the results for small metallic clusters to infinite substrates. Even in semiconductor systems such as Si where the convergence of the results with respect to the cluster size should be much faster than for metals because of the more localized nature of the molecular orbitals, clusters of 27 atoms are not sufficient to reproduce the results of slab calculations quantitatively.[44,49]

Furthermore, we have to admit that our results for the system O_2/Al_{22} still have to be taken with caution because of the difficulties associated with obtaining well-converged results. Furthermore, the basis set used in the O_2/Al_{22} calculations is

also rather small. It should furthermore be mentioned that the DFT description of O_2 is not very accurate. Using the PBE functional within an all-electron approach leads to an O_2 binding energy that is about 1 eV larger than the experimental value.[12,13] However, recall that there is also a deviation of 0.3 eV in the dioxygen binding energy between experiment and theory at the MCI level because of the limited (TZ) basis set used.

In addition, recently it was found that the B3LYP functional gives a poor description of metal properties,[50] as other hybrid functionals also do.[43] Hence, the B3LYP O_2/Al_{22} results might not be reliable. Considering all of these uncertainties, we conclude that this study can certainly not give a definite answer. It is clear that spin effects play an important role in the O_2/Al system, as the recent experiments on small Al anion clusters confirm.[27] Light elements with a weak spin−orbit coupling and a low density of states at the Fermi level such as Al do not readily induce spin transitions in impinging atoms and molecules, as a recent electronically nonadiabatic dynamical study of the interaction of atomic hydrogen with Al(111) employing time-dependent DFT demonstrated.[51] The delayed spin flip leads to an electronically excited state and thus to an effective additional reaction barrier. This mechanism will most probably be operative in the O_2/Al system, even if there is a non-vanishing dissociative adsorption barrier in the electronic ground state. Nevertheless, our study clearly shows that the correct treatment of electronic many-body effects is crucial for the accurate determination of the adsorption barrier in the O_2/Al system and that the origin of the discrepancy between experiment and periodic DFT calculations with respect to the existence of an adsorption barrier in the system O_2/Al(111) certainly deserves further studies on a higher level of theory, for example with improved, more realistic density functionals.

Acknowledgment. This work has been supported by the joint IKYDA programme of the German Academic Exchange Service (DAAD) and the Greek State Scholarships Foundation (I.K.Y.).

References and Notes

(1) Freund, H.-J. *Surf. Sci.* **2002**, *500*, 271.
(2) Nolan, P. D.; Lutz, B. R.; Tanaka, P. L.; Davis, J. E.; Mullins, C. B. *J. Chem. Phys.* **1999**, *111*, 3696.
(3) Gross, A.; Eichler, A.; Hafner, J.; Mehl, M. J.; Papaconstantopoulos, D. A. *J. Chem. Phys.* **2006**, *124*, 174713.
(4) Österlund, L.; Zorić, I.; Kasemo, B. *Phys. Rev. B* **1997**, *55*, 15452−15455.
(5) Brune, H.; Wintterlin, J.; Behm, R. J.; Ertl, G. *Phys. Rev. Lett.* **1992**, *68*, 624.
(6) Sasaki, T.; Ohno, T. *Surf. Sci.* **1999**, *433*, 172.
(7) Honkala, K.; Laasonen, K. *Phys. Rev. Lett.* **2000**, *84*, 705.
(8) Yourdshahyan, Y. Y.; Razaznejad, B.; Lundqvist, B. I. *Phys. Rev. B* **2002**, *65*, 075416.
(9) Behler, J.; Delley, B.; Lorenz, S.; Reuter, K.; Scheffler, M. *Phys. Rev. Lett.* **2005**, *94*, 036104.
(10) Behler, J.; Delley, B.; Reuter, K.; Scheffler, M. *Phys. Rev. B* **2007**, *75*, 115409.
(11) Perdew, J. P.; Burke, K.; Ernzerhof, M. *Phys. Rev. Lett.* **1996**, *77*, 3865.
(12) Hammer, B.; Hansen, L. B.; Nørskov, J. K. *Phys. Rev. B* **1999**, *59*, 7413.
(13) Lischka, M.; Mosch, C.; Gross, A. *Electrochim. Acta* **2007**, *52*, 2219.
(14) Castleman, A. W., Jr.; Jena, P. *Proc. Natl. Acad. Sci.* **2006**, *103*, 10554.
(15) Leuchtner, R. E.; Harms, A. C.; Castleman, A. W. *J. Chem. Phys.* **1991**, *94*, 1093.
(16) Ruatta, S. A.; Hanley, L.; Aanderson, S. L. *Chem. Phys. Lett.* **1987**, *137*, 5.
(17) Cooper, B. T.; Parent, D.; Buckner, S. W. *Chem. Phys. Lett.* **1998**, *284*, 401.
(18) Wu, H.; Li, X.; Wang, X.-B.; Ding, C.-F.; Wang, L.-S. *J. Chem. Phys.* **1998**, *109*, 449.
(19) Burgert, R.; Schnöckel, H.; Olzmann, M.; Bowen, K. H., Jr. *Angew. Chem., Int. Ed.* **2006**, *45*, 1476.
(20) Jones, R. O. *J. Chem. Phys.* **1993**, *99*, 1194.
(21) Rao, B. K.; Jena, P. *J. Chem. Phys.* **1999**, *111*, 1890.
(22) Ueno, J.; Hoshino, T.; Hata, M.; Tsuda, M. *Appl. Surf. Sci.* **2000**, *162*, 440.
(23) Martínez, A.; Tenorio, F. J.; Ortiz, J. V. *J. Phys. Chem. A* **2003**, *107*, 2589.
(24) Sun, J.; Lu, W. C.; Wang, H.; Li, Z.-S.; Sun, C.-C. *J. Phys. Chem. A* **2006**, *110*, 2729.
(25) Boldyrev, A. I.; Wang, L. S. *Chem. Rev.* **2005**, *105*, 3716.
(26) Hu, X.; Li, H.; Wang, C.; Han, S. *Chem. Phys. Lett.* **2006**, *426*, 39.
(27) Burgert, R.; Schnöckel, H.; Grubisic, A.; Li, X.; Bowen, S. T. S. K. H.; Ganteför, G. F.; Kiran, B.; Jena, P. *Science* **2008**, *319*, 438.
(28) Hoshino, T.; Sekino, A.; Hata, M.; Tsuda, M. *Appl. Surf. Sci.* **2000**, *162*, 435.
(29) Campbell, T.; Kalia, R. K.; Nakano, A.; Vashishta, P.; Ogata, S.; Rodgers, S. *Phys. Rev. Lett.* **1999**, *82*, 4866−4869.
(30) *MOLPRO 2000* is a package of ab initio programs designed by H.-J. Werner and P. J. Knowles, version 2002.6, R. D. Amos, A. Bernhardsson, A. Berning, P. Celani, D. L. Cooper, M. J. O. Deegan, A. J. Dobbyn, F. Eckert, C. Hampel, G. Hetzer, P. J. Knowles, T. Korona, R. Lindh, A. M. Lloyd, S. J. McNicholas, F. R. Manby, W. Meyer, M. E. Mura, A. Nicklass, P. Palmieri, R. Pitzer, G. Rauhut, M. Schütz, U. Schumann, H. Stoll, A. J. Stone, R. Tarroni, T. Thorsteinsson, and H. -J. Werner.
(31) Frisch, M. J.; Trucks, G. W.; Schlegel, H. B.; Scuseria, G. E.; Robb, M. A.; Cheeseman, J. R.; Montgomery, J. A., Jr.; Vreven, T.; Kudin, K. N.; Burant, J. C.; Millam, J. M.; Iyengar, S. S.; Tomasi, J.; Barone, V.; Mennucci, B.; Cossi, M.; Scalmani, G.; Rega, N.; Petersson, G. A.; Nakatsuji, H.; Hada, M.; Ehara, M.; Toyota, K.; Fukuda, R.; Hasegawa, J.; Ishida, M.; Nakajima, T.; Honda, Y.; Kitao, O.; Nakai, H.; Klene, M.; Li, X.; Knox, J. E.; Hratchian, H. P.; Cross, J. B.; Bakken, V.; Adamo, C.; Jaramillo, J.; Gomperts, R.; Stratmann, R. E.; Yazyev, O.; Austin, A. J.; Cammi, R.; Pomelli, C.; Ochterski, J. W.; Ayala, P. Y.; Morokuma, K.; Voth, G. A.; Salvador, P.; Dannenberg, J. J.; Zakrzewski, V. G.; Dapprich, S.; Daniels, A. D.; Strain, M. C.; Farkas, O.; Malick, D. K.; Rabuck, A. D.; Raghavachari, K.; Foresman, J. B.; Ortiz, J. V.; Cui, Q.; Baboul, A. G.; Clifford, S.; Cioslowski, J.; Stefanov, B. B.; Liu, G.; Liashenko, A.; Piskorz, P.; Komaromi, I.; Martin, R. L.; Fox, D. J.; Keith, T.; Al-Laham, M. A.; Peng, C. Y.; Nanayakkara, A.; Challacombe, M.; Gill, P. M. W.; Johnson, B.; Chen, W.; Wong, M. W.; Gonzalez, C.; Pople, J. A. *Gaussian 03*, revision C.02; Gaussian, Inc.: Wallingford, CT, 2004.
(32) Kresse, G.; Furthmüller, J. *Phys. Rev. B* **1996**, *54*, 11169.
(33) Woon, D.; Dunning, T., Jr. *J. Chem. Phys.* **1993**, *98*, 1358.
(34) Herzberg, G.; Huber, K. P. *Molecular Spectra and Molecular Structure. IV. Constants of Diatomic Molecules*; Van Nostrand Reinhold: New York, 1979.
(35) Martínez, A.; Vela, A. *Phys. Rev. B* **1994**, *49*, 17464.
(36) Martínez, A.; Vela, A.; Salahub, D. R.; Calaminici, P.; Russo, N. *J. Chem. Phys.* **1994**, *101*, 10677.
(37) McLean, A. D.; Chandler, G. S. *J. Chem. Phys.* **1980**, *72*, 5639.
(38) Becke, A. D. *J. Chem. Phys.* **1993**, *98*, 5648.
(39) Lee, C.; Yang, W.; Parr, R. *Phys. Rev. B* **1988**, *37*, 785.
(40) Blöchl, P. E. *Phys. Rev. B* **1994**, *50*, 17953.
(41) Kresse, G.; Joubert, D. *Phys. Rev. B* **1999**, *59*, 1758.
(42) Moseler, M.; Häkkinen, H.; Barnett, R. N.; Landman, U. *Phys. Rev. Lett.* **2001**, *86*, 2545.
(43) Paier, J.; Marsman, M.; Hummer, K.; Kresse, G.; Gerber, I. C.; Ángyán, J. G. *J. Chem. Phys.* **2006**, *124*, 154709.
(44) Filippi, C.; Healy, S. B.; Kratzer, P.; Pehlke, E.; Scheffler, M. *Phys. Rev. Lett.* **2002**, *89*, 166102.
(45) Tuma, C.; Sauer, J. *Phys. Chem. Chem. Phys.* **2006**, *8*, 3955.
(46) Hu, Q.-M.; Reuter, K.; Scheffler, M. *Phys. Rev. Lett.* **2007**, *98*, 176103.
(47) Hu, Q.-M.; Reuter, K.; Scheffler, M. *Phys. Rev. Lett.* **2007**, *98*, 169903(E).
(48) Kresse, G.; Gil, A.; Sautet, P. *Phys. Rev. B* **2003**, *68*, 073401.
(49) Penev, E.; Kratzer, P.; Scheffler, M. *J. Chem. Phys.* **1999**, *110*, 3986.
(50) Paier, J.; Marsman, M.; Kresse, G. *J. Chem. Phys.* **2007**, *127*, 024103.
(51) Lindenblatt, M.; Pehlke, E. *Phys. Rev. Lett.* **2006**, *97*, 216101.